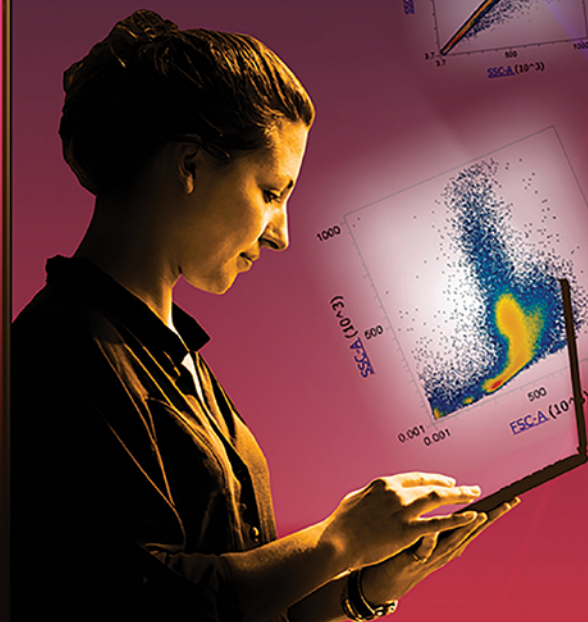
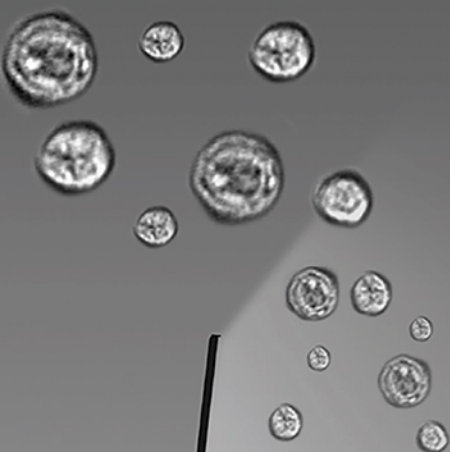


invitrogen

Two data sets. One step. Zero doubt.



Confidently confirm your cell profiles with a new flow cytometer that delivers flow cytometry and imaging data simultaneously. Now, you can acquire dual data quickly and easily. The new Invitrogen™ Attune™ CytPix™ Flow Cytometer delivers both brightfield images and flow cytometry data sets simultaneously, so you can confirm cellular characteristics and sample quality confidently, without changing your protocols.




Enhance analysis and confidence at [thermofisher.com/cytpix](https://www.thermofisher.com/cytpix)

ThermoFisher
SCIENTIFIC

For Research Use Only. Not for use in diagnostic procedures. © 2021 Thermo Fisher Scientific Inc. All rights reserved. All trademarks are the property of Thermo Fisher Scientific and its subsidiaries unless otherwise specified. COL25211 0621

Short Communication

Plasma membrane Ca^{2+} ATPase 1 (PMCA1) but not PMCA4 is critical for B-cell development and Ca^{2+} homeostasis in mice

Mark Korthals¹, Laura Tech¹, Kristina Langnaese¹, Anna Gottfried¹, Johannes Hradsky¹, Ulrich Thomas², Ana Claudia Zenclussen³, Monika C. Brunner-Weinzierl⁴, Kerry Tedford^{*1} and Klaus-Dieter Fischer^{*1} 

¹ Institute for Biochemistry and Cell Biology, Otto-von-Guericke University, Magdeburg, Germany

² Department of Neurochemistry and Molecular Biology, Leibniz Institute for Neurobiology, Magdeburg, Germany

³ Experimental Obstetrics and Gynecology, Otto-von-Guericke University, Magdeburg, Germany

⁴ Department of Pediatrics, Otto-von-Guericke University, Magdeburg, Germany

The amplitude and duration of Ca^{2+} signaling is crucial for B-cell development and self-tolerance; however, the mechanisms for terminating Ca^{2+} signals in B cells have not been determined. In lymphocytes, plasma membrane Ca^{2+} ATPase (PMCA) isoforms 1 and 4 (PMCA1 and PMCA4, aka ATP2B1 and ATP2B4) are the main candidates for expelling Ca^{2+} from the cell through the plasma membrane. We report here that *Pmca4* (*Atp2b4*) KO mice had normal B-cell development, while mice with a conditional KO of *Pmca1* (*Atp2b1*) had greatly reduced numbers of B cells, particularly splenic follicular B cells, marginal zone B cells, and peritoneal B-1a cells. Mouse and naïve human B cells showed only PMCA1 expression and no PMCA4 by western blot, in contrast to T cells, which did express PMCA4. Calcium handling was normal in *Pmca4*^{-/-} B cells, but *Pmca1* KO B cells had elevated basal levels of Ca^{2+} , elevated levels in ER stores, and reduced Ca^{2+} clearance. These findings show that the PMCA1 isoform alone is required to ensure normal B-cell Ca^{2+} signaling and development, which may have implications for therapeutic targeting of PMCA and Ca^{2+} in B cells.

Keywords: B cells · Ca^{2+} · PMCA1 · PMCA4 · development



Additional supporting information may be found online in the Supporting Information section at the end of the article.

Introduction

B-cell receptor (BCR) signaling thresholds are tightly regulated during development to ensure that signal strength is sufficient

for positive selection yet not as high as would be induced by an auto-reactive BCR encountering self-antigen. This tight control of signaling requires precise adjustment of changes to cytosolic Ca^{2+} concentration, and consequently mutations in proteins

Correspondence: Dr. Klaus-Dieter Fischer
e-mail: klaus.fischer@med.ovgu.de

*These are senior authors.

that affect Ca^{2+} levels are often associated with autoimmune disease [1]. Cytosolic Ca^{2+} levels are maintained in a balance with stored levels in organelles by channels and pumps including sarco/endoplasmic reticulum Ca^{2+} ATPases (SERCAs) that transfer Ca^{2+} to the endoplasmic reticulum (ER) and by plasma membrane Ca^{2+} ATPases (PMCA) that expel Ca^{2+} outside the cell through the plasma membrane [2, 3]. PMCA activity is regulated by multiple mechanisms, many converging on the C-terminal tail that mediates binding to proteins that localize it to specific microdomains and that inhibits ATPase activity until released by Ca^{2+} -bound calmodulin [4, 5]. In humans, PMCA is associated with cardiovascular disease, hypertension, and malaria resistance [6].

PMCA consists of four isoforms, PMCA1–4: PMCA1 is expressed in a wide range of tissues, PMCA2 and PMCA3 are largely expressed in the nervous system, and PMCA4 expression is less broad than PMCA1 and may be controlled by differentiation [6]. PMCA isoforms are also variably expressed during development according to requirements for Ca^{2+} signal strength and duration [2–7]. As a result, diseases due to PMCA mutations are isoform specific. In mice, a complete deletion of PMCA1 is lethal, but deletions of PMCA2, 3, and 4 induce diseases including deafness, ataxia, and sterility [6]. Both PMCA1 and PMCA4 are expressed in mouse T cells [8]. Moreover, in human Jurkat T cells, PMCA4 is the leading isoform for calcium clearance and NFAT transcriptional activity [9]. However, mouse B cells can differ from T cells in their requirements for various Ca^{2+} handling proteins; for example, the mitochondrial Na^{+} - Ca^{2+} exchanger NCLX is required for B-cell migration but not T-cell migration [10]. Therefore, identifying which PMCA isoforms are present in B cells is necessary for specifically targeting those isoforms for therapeutic benefit. In mouse B cells, one study reported that PMCA4 negatively regulates BCR signaling to Ca^{2+} clearance by associating with CD22 [11]. Here, we compare the roles of PMCA1 and PMCA4 in B cells and report that PMCA1 is the main isoform expressed in B cells and that reductions in PMCA1 compromised B-cell development and Ca^{2+} efflux.

Results and discussion

B-cell development requires the PMCA1 isoform but not PMCA4

We previously showed that neuroplastin is a chaperone-like molecule required for PMCA stability, and T cells lacking neuroplastin have a profound reduction in both PMCA1 and PMCA4 leading to failures in Ca^{2+} clearance and NFAT signaling [8]. We wanted to extend these studies to the roles of PMCA in B cells; therefore, we first compared the effects of loss of either *Pmca1* or *Pmca4* on B-cell development. Surprisingly, *Pmca4* knockout (KO) B cells were present in normal numbers in every population in the BM, spleen, and peritoneal cavity, with the exception of a reduction in peritoneal B-1b cells (Fig. 1A). Similarly,

mice with a heterozygous B-cell-specific mutation of the *Pmca1* gene, *Pmca1^{f/f} CD19-Cre⁺* mice, also had normal B-cell development, with only a slight reduction in B-1 cells that may be due to CD19-Cre effects [12] (Fig. 1B). In contrast, mice with a homozygous conditional KO (cko) of *Pmca1* in B cells, *Pmca1^{f/f} CD19-Cre⁺* mice, showed strongly decreased numbers and relative proportions for most populations subsequent to early pre-pro B cells and in splenic follicular B cells (FOBs), although marginal zone B cell (MZB) numbers were normal (Fig. 1C). In the peritoneum, B-1a cells in particular showed a strong relative reduction (Fig. 1C). Gating strategies and representative flow cytometric plots are shown in Fig. 1D and Supporting Information Fig. 1. Thus, peripheral B-cell differentiation requires PMCA1 but not PMCA4.

Comparison of PMCA1 and PMCA4 expression in T and B cells

Using western blots, we were unable to detect PMCA4 protein in B-cell lysates from either WT or *Pmca4* KO mice (Fig. 2A). PMCA4 was found in T-cell lysates and in total splenocyte lysates from WT but not *Pmca4* KO mice, confirming the specificity of the PMCA4 antibody (Fig. 2A). We next checked expression of PMCA1 in lysates from control and from *Pmca1* cko B cells mice and observed that the *CD19-Cre*-mediated deletion of *Pmca1* was inefficient [12–15], as PMCA1 expression was reduced but not completely absent (Fig. 2B). The remaining PMCA1 expression suggested that WT B cells were still present. Using genomic PCR, we confirmed the presence of WT configuration alleles (with Flip and LoxP sites at the *Pmca1* locus) along with Cre-deleted *Pmca1* alleles (Supporting Information Fig. 2A–C). The ratio of *Pmca1* cko to WT configuration alleles increased gradually in BM B cells subsets and paralleled development, likely due to the increased CD19 expression during development [12, 15]. One exception was noted in MZBs as there was a decrease in the proportion of *Pmca1* cko alleles in this population compared to FOBs, indicating that there was a strong selection against the *Pmca1* mutation in MZBs (Supporting Information Fig. 2C).

PMCA1 was clearly detected in all human cell lines, but PMCA4 signals were only strong in Jurkat T cells and Raji lymphoma B cells and were present at relatively low levels in Ramos and BJAB B-cell lines. The results from primary human naïve B cells were consistent with mouse B cells, as only PMCA1 protein was detected in the lysates and not PMCA4. A slight amount of PMCA4 was detectable in human memory B cells, possibly due to upregulation of PMCA4 during B-cell differentiation (Fig. 2C, Supporting Information Fig. 2D). A PCR analysis of the relative levels of *Pmca1* and *Pmca4* mRNA showed only trace amounts of *Pmca4* and markedly stronger levels of *Pmca1* mRNA in B cells, in line with the western blot results (Fig. 2D and E). Together, these data show that mouse and human B cells differ from T cells in that they express substantially less PMCA4 and a much higher proportion of PMCA1.

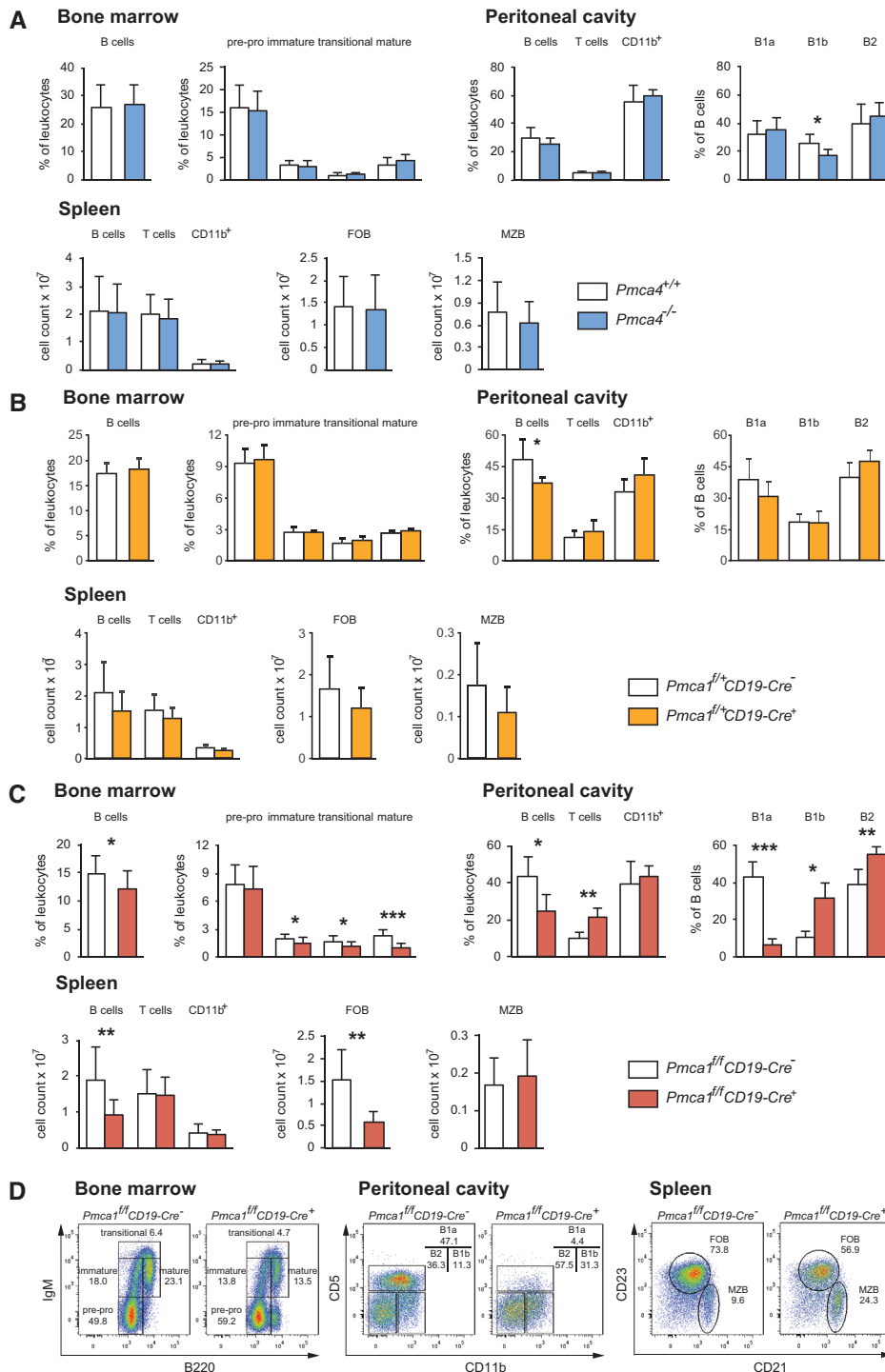


Figure 1. PMCA1 alone and not PMCA4 is required for B-cell development. Flow cytometry analysis of leukocytes isolated from bone marrow (BM), peritoneum (PC), and spleen (S) of (A) WT and $Pmca4^{-/-}$ mice, (B) $Pmca1^{fl/fl}CD19-Cre^+$ and Cre^- controls, and (C) $Pmca1^{fl/fl}CD19-Cre^+$ and Cre^- controls. Indicated leukocyte populations were gated as shown in Supporting Information Fig. 1A and B. Mean frequencies or absolute numbers of cell populations \pm SD were derived from the indicated numbers of individual mice and independent experiments: (A) BM: six versus eight mice pooled from four experiments; PC: five versus six mice pooled from three experiments; S B, T, and $CD11b^+$ cells: six versus eight mice pooled from four experiments; S FOB and MZB: five versus six mice pooled from three experiments and (B) BM: 14 versus 13 mice pooled from six experiments; PC: five versus four mice pooled from three experiments; S B and $CD11b^+$ cells: 12 versus 11 mice pooled from six experiments; S T cells: seven versus seven mice pooled from four experiments; S FOB and MZB: nine versus eight mice from four experiments. (C) BM: four versus four mice pooled from three experiments; PC: six versus six mice pooled from five experiments; S: four versus four mice pooled from three experiments. Student's t-test, * $p < 0.05$. (D) Representative flow cytometry plots illustrate the relative differences in B-cell subpopulations of controls ($Pmca1^{fl/fl}CD19-Cre^-$) and $Pmca1^{fl/fl}CD19-Cre^+$ mice. Inset numbers indicate percentages of total B cells. Student's t-test, * $p < 0.05$, ** $p < 0.01$, *** $p < 0.001$.

PMCA1 promotes B cell Ca^{2+} clearance

To test the extent of PMCA involvement in Ca^{2+} extrusion in B cells, we compared Ca^{2+} entry and clearance using a flow cytometric store-operated calcium entry (SOCE) protocol [8, 16] (typical WT B cell trace shown in Fig. 3A). Addition of thapsigargin (Tg) depletes Ca^{2+} stores in the ER by irreversibly inhibiting SERCA pumps, resulting in an increase in cytosolic Ca^{2+} ($[Ca^{2+}]_i$)

before levels return to baseline. Subsequent addition of Ca^{2+} then causes a large increase in $[Ca^{2+}]_i$ via store-operated opening of ORAI1 channels, and a stable plateau of the $[Ca^{2+}]_i$ trace is established due to simultaneous influx and extrusion of Ca^{2+} . Removal of extracellular Ca^{2+} stops the Ca^{2+} influx, resulting in a biphasic fast and slow response of Ca^{2+} clearance (Fig. 3A).

To test the requirement for PMCA in Ca^{2+} clearance in B cells, we added sodium orthovanadate (Na_3VO_4), an inhibitor of

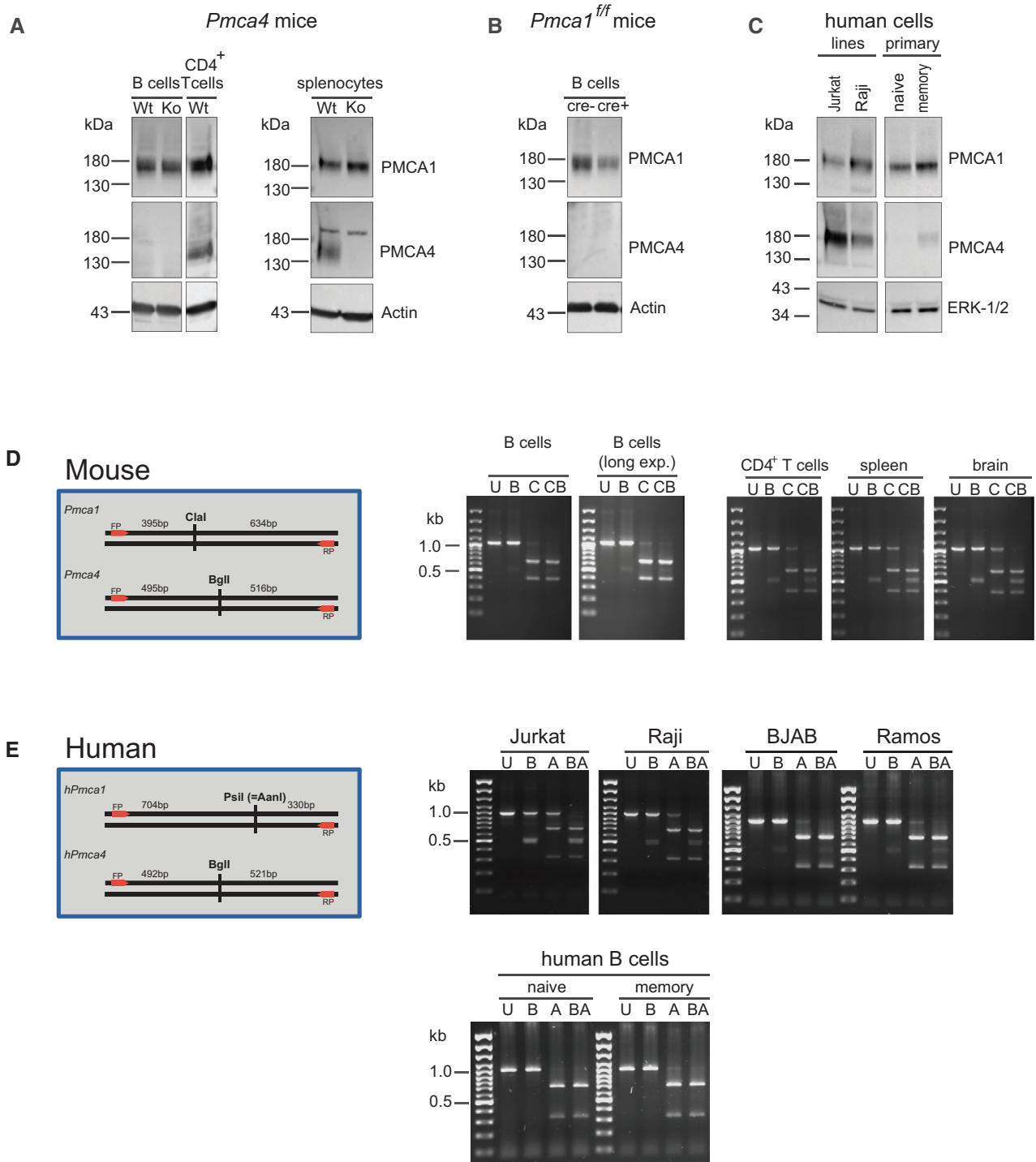


Figure 2. Specific expression of PMCA1 versus PMCA4 in B cells. (A and B) Lysates (30 μ g/lane) from (A) WT and *Pmca4*^{-/-} B cells (n = 10 and 4), WT CD4⁺ T cells (n = 4), WT and *Pmca4*^{-/-} splenocytes (n = 4 each), and (B) *Pmca1*^{ff} CD19-Cre⁺ and Cre⁻ control B cells (n = 4 each) were immunoblotted for PMCA1, PMCA4, and actin as loading controls. (C) Lysates (30 μ g/lane) from Jurkat and Raji cell lines (n = 4 each) and from purified human naive and memory B cells (n = 4) were blotted as in (A) with ERK1/2 as a loading control. One representative image from three independent experiments for (A), two experiments for (B), and two experiments for (C) is shown. (D and E) Relative mRNA expression levels of *Pmca1* and *Pmca4* isoforms in murine B cells (D) and human B cells (E) were analyzed by RT-PCR using the relative PCR strategy (diagrams, left) showing the set of PCR primers (forward primer, FP; reverse primer, RP) used to amplify a 1 kb region from both *Pmca1* and *Pmca4* cDNA. (D) The resulting PCR products were digested with ClaI (C), BgII (B), both (CB) or neither (uncut, U), yielding two \sim 0.4 and \sim 0.6 kb fragments for *Pmca1* and two \sim 0.5 fragments for *Pmca4*. Fragments were subsequently separated by electrophoresis (n = 5 from 5 experiments). For B cells, an additional image of a longer exposure of the gel shows some *Pmca4* product. (E) Relative PCR as in (D) but with the indicated human cell lines and primary human B cells. PCR fragments were digested with PstI/AanI (A) and BgII (B), both (AB), or neither (uncut, U), yielding two fragments of \sim 0.7 and \sim 0.3 kb for *Pmca1* and two \sim 0.5 fragments for *Pmca4* (n = 2 from two experiments).

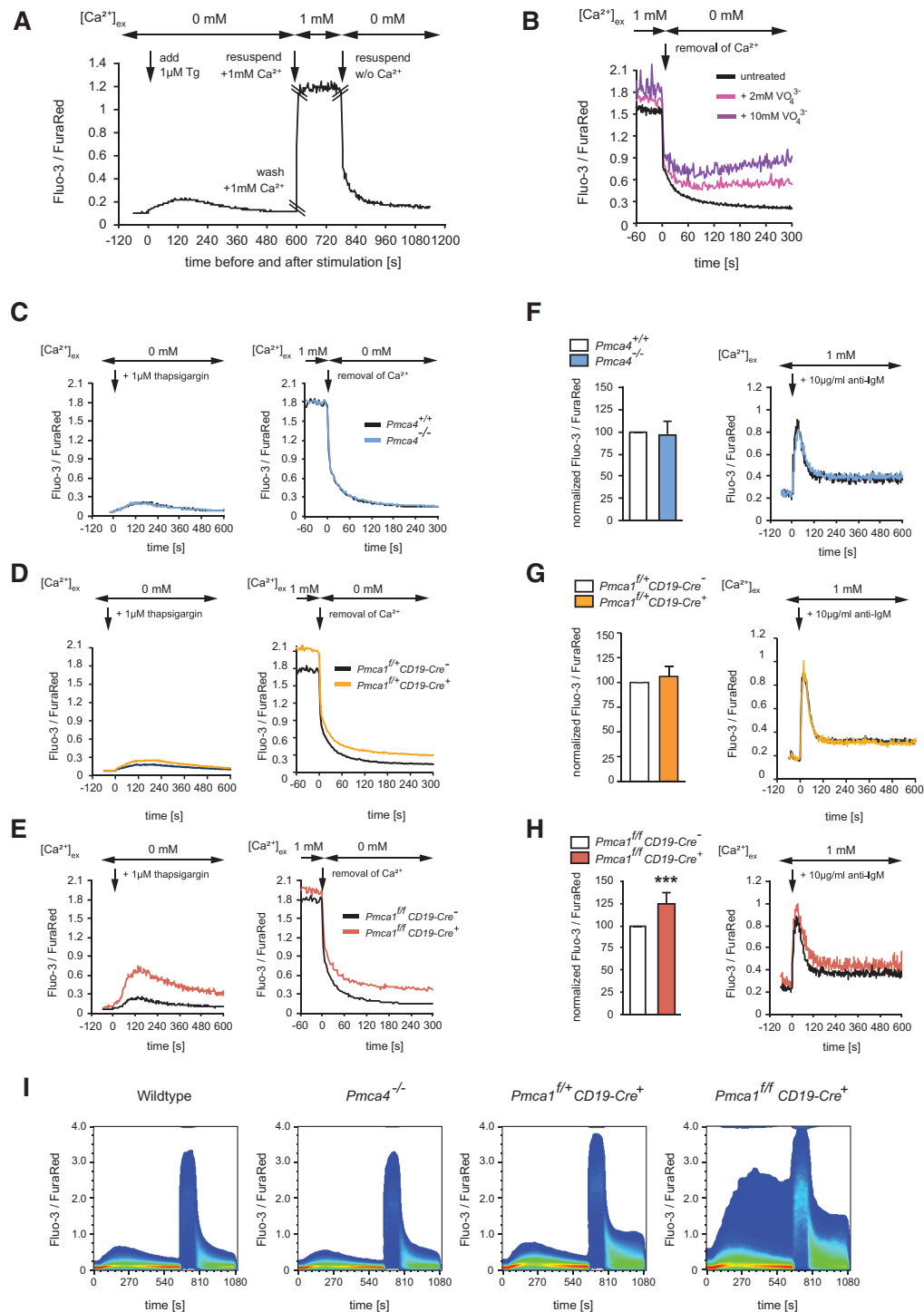


Figure 3. Roles for PMCA1 in B-cell calcium clearance. Cytosolic Ca^{2+} levels in follicular B cells (FOBs) labeled with Ca^{2+} -sensitive dyes Fluo-3 and FuraRed measured by ratiometric flow cytometry. (A) Diagram showing complete kinetics of SOCE experiment in WT FOBs; see text for details. (B) Ca^{2+} clearance after SOCE in the absence of SERCAs from 1 min before Ca^{2+} removal, as shown in diagram in (A), in WT FOBs treated with PMCA blocking reagent VO_4^{3-} at 2 mM or 10 mM (representative plot from three independent experiments with one WT mouse per experiment). (C–E) Depletion of Ca^{2+} from ER stores by treatment with 1 μM thapsigargin (Tg) to block SERCAs in the absence of extracellular Ca^{2+} (left panel) and Ca^{2+} clearance after SOCE (right panel), as shown in diagram in (A). (F–H) Bar graph of baseline cytosolic Ca^{2+} levels show mean \pm SD of Fluo-3/FuraRed ratios normalized to the corresponding WT value in each experiment (left) and representative trace of Ca^{2+} kinetics with 10 $\mu\text{g}/\text{mL}$ anti-IgM F(ab')₂ in the presence of 1 mM extracellular Ca^{2+} (right panel). Student's t-test, *** $p < 0.001$. (C and F) WT and *Pmca4*^{-/-} FOBs (one representative experiment of five for release of ER Ca^{2+} , one representative experiment of five for Ca^{2+} clearance, mean \pm SD from six experiments for baseline Ca^{2+} , one representative experiment of six for BCR-induced Ca^{2+} ; $n = 1$ mouse per genotype in each experiment). (D, and G) Control (*Pmca1*^{fl/fl} CD19-Cre⁻) and *Pmca1*^{fl/fl} CD19-Cre⁺ FOBs (one representative experiment of five for depletion of ER Ca^{2+} , one representative experiment of three for Ca^{2+} clearance,

phosphate-dependent enzymes such as phosphatases and PMCA. We observed a strong decrease in Ca^{2+} clearance from B cells in a dose-dependent manner (Fig. 3B), accompanied by cells with extremely high $[\text{Ca}^{2+}]_i$ (Supporting Information Fig. 4D), demonstrating the importance of PMCA to Ca^{2+} clearance. In *Pmca4* KO B cells, all Ca^{2+} signals were normal including Ca^{2+} release from intracellular stores and the activation of Ca^{2+} clearance (Fig. 3C), as well as basal $[\text{Ca}^{2+}]_i$ and BCR-activated $[\text{Ca}^{2+}]_i$ (Fig. 3F and Supporting Information Fig. 3B). Additionally, in heterozygous *Pmca1^{f/+} CD19-Cre⁺* B cells, Ca^{2+} release from intracellular stores was modestly elevated and Ca^{2+} clearance was reduced (Fig. 3D) but basal and IgM-induced Ca^{2+} were normal (Fig. 3G and Supporting Information Fig. 3C). In comparison, Ca^{2+} was strongly affected in *Pmca1* cko B cells, with greatly increased Ca^{2+} levels in ER stores and reduced Ca^{2+} clearance after SOCE (Fig. 3E) and increases in basal $[\text{Ca}^{2+}]_i$ and in BCR-activated $[\text{Ca}^{2+}]_i$ (Fig. 3H and Supporting Information Fig. 3D). Interestingly, the strongly increased $[\text{Ca}^{2+}]_i$ following Tg in *Pmca1* cko cells (Fig. 3E) suggests that the SERCA pumps were able to counteract the increased $[\text{Ca}^{2+}]_i$ in the cko cells by storing it in the ER. This Ca^{2+} removal by the SERCAs from the cytoplasm may keep the cko cells alive longer, as prolonged high levels of Ca^{2+} are cytotoxic and may cause cell death during the SOCE assay.

We also tested Ca^{2+} in separate B-cell subsets from *Pmca1* cko mice, and found that $[\text{Ca}^{2+}]_i$ was elevated in all subsets and so was not specific to any stage of development (Supporting Information Fig. 3F–G), with one exception. In splenic MZBs, $[\text{Ca}^{2+}]_i$ levels were not as increased as in the other subsets, and the response to Tg was only slightly elevated (Supporting Information Fig. 3A and E). These findings are consistent with the genomic PCR that showed a higher proportion of WT configuration MZB cells in the *Pmca1* cko B cells (Supporting Information Fig. 2C), indicating that the $[\text{Ca}^{2+}]_i$ levels were almost normal because there were more WT B cells in the subset. Thus, the high Ca^{2+} levels in the other subsets from *Pmca1* cko mice correlate with lack of PMCA1 expression. Flow cytometry density plots of $[\text{Ca}^{2+}]_i$ in single *Pmca1* cko B cells also show a higher fraction of cells with extreme $[\text{Ca}^{2+}]_i$ upon Tg treatment and after SOCE when compared to WT, *Pmca4^{-/-}*, or heterozygous *Pmca1^{f/+} CD19-Cre⁺* B cells (Fig. 3I), and similar to WT B cells treated with high doses of VO_4^{3-} (Supporting Information Fig. 4D). We quantified the frequency of *Pmca1* cko FOBs that showed extreme $[\text{Ca}^{2+}]_i$ upon Tg treatment (Supporting Information Fig. 4A–C) and found that there was about a five- to tenfold increase in these cells in *Pmca1* cko samples compared to controls (Supporting Information Fig. 4C). Together, these data show that PMCA1 is essential for restraining Ca^{2+} levels in B cells while PMCA4 is not.

Concluding remarks

Here, we characterized expression of PMCA isoforms and found that PMCA1 is the main isoform in mouse and human B cells and is required for normal mouse B-cell development and for inhibiting Ca^{2+} levels. We used the CD19-Cre system to analyze *Pmca1* cko B cells because CD19 expression rises throughout B-cell development, thus relatively inefficient deletion in earlier B cell stages allows for development of PMCA1⁺ cells that progress to subsequent stages. Loss of PMCA1 affected all B-cell subsets but in particular MZB cells and B-1a cells. These observations are supported by the “strength of signaling” model for the role of BCR signaling in the development of FOB and MZB cells [17, 18]. This model predicts that only MZB precursors with BCR that is weakly reactive to self-antigen will become MZB cells, while intermediate signaling through BCR would lead to FOBs, and strong BCR signals to B-1 cells. As *Pmca1* cko MZB precursors would have higher levels of Ca^{2+} signaling, they would not be selected as mature MZBs. The WT configuration MZBs present in the mix would then expand to fill the MZB niche [18, 19], supporting our genomic PCR finding of more WT configuration alleles in the MZBs and an almost normal Ca^{2+} phenotype. Moreover, *Pmca1* cko mice lack B-1a cells while B-1b cells are present. B-1b cells represent the activated form of B-1a cells [20]. The high levels of intracellular Ca^{2+} in *Pmca1* cko B-1 cells may lead to increased activation of the cells, subsequent downregulation of CD5, and the switch to the CD5⁻ B-1b cells.

In contrast to a previous study reporting that PMCA4 is active in B cells [11], we found no protein expression of PMCA4 in mouse B cells and no defect in Ca^{2+} clearance in *Pmca4^{-/-}* B cells. However, we do not rule out a potential role for PMCA4 in BCR-induced differentiation of B cells, which would require strong BCR activation to achieve sustained levels of cytosolic Ca^{2+} signaling and then possibly a specific isoform of PMCA to shape and reduce it. This would be consistent with our finding that human memory B cells and lymphoma cells express low levels of PMCA4, with ImmGen data [21], and with previous reports that PMCA4 expression is upregulated during differentiation of cancer cell lines and in B cells from chronic lymphocytic leukemia patients [22–24]. In Jurkat T cells and in a mouse B-cell line, Ca^{2+} clearance is achieved only through PMCA, with no contribution from the Na^+ - Ca^{2+} exchanger NCX [11, 16]. Given that we found no PMCA4 in primary mouse B cells, a lack of NCX would mean that PMCA1 is the sole mechanism for Ca^{2+} extrusion. Interestingly, B cells with knockouts of key regulators of SOCE—STIM1 and STIM2, or ORAI1—have severe defects in SOCE and BCR signaling to NFAT, but still develop normally [25, 26]. We show here, though, that *Pmca1* cko B cells do not develop

mean \pm SD from four experiments for baseline Ca^{2+} , one representative experiment of four for BCR-induced Ca^{2+} ($n = 1$ mouse per genotype in each experiment). (E and H) Control (*Pmca1^{f/f} CD19-Cre⁻*) and *Pmca1^{f/f} CD19-Cre⁺* FOBs (one representative experiment of ten for release of ER Ca^{2+} , one representative experiment of four for Ca^{2+} clearance, mean \pm SD from seven experiments for baseline Ca^{2+} , one representative experiment of seven for BCR-induced Ca^{2+} ; $n = 1$ mouse per genotype in each experiment). (I) Representative pseudocolor density plots of Ca^{2+} kinetics as described in (A) illustrating distribution of single B cells (>500 000 each) with varying Ca^{2+} loads from mice of indicated genotypes.

normally, suggesting that developing B cells must keep Ca^{2+} levels relatively low by refraining from SOCE and by expressing PMCA1.

Materials and methods

Mouse and cell lines

Pmca1^{f/f} (*Atp2b1^{tm1c}*) mice were generated from C57BL/6 ES cells provided by UC Davis Knockout Mouse Project (www.komp.org; project ID CSD77635) as described [8]. *CD19-Cre⁺* mice were previously described and on a C57BL/6 background¹¹. *Pmca4^{-/-}* (*Atp2b4*) mice [27] (MMRRC stock #36807) and corresponding WT controls were on a FVB/N background. All mouse studies were approved by the Landesverwaltungsamt Halle, Germany (representing the state of Saxony-Anhalt) (License: 2–1181). Jurkat T cells, Raji, Ramos, and BJAB cell lines were from ATCC.

Lymphocyte preparation and flow cytometry

Mouse T and B cells were prepared as described [8]. For Western blots, splenic T cells and B cells were enriched using the MACS CD4⁺ T cell isolation kit and CD43 microbeads, respectively (MACS; Miltenyi Biotec). Human PBMCs were obtained from healthy volunteers and isolated using a leukocyte reduction filter (Sepacell RZ-2000; Asahi Kasei Medical) supplied by the Institute of Transfusions Medicine (University Hospital of Magdeburg). Experiments were approved by the Ethics Committee of the Otto-von-Guericke University (EK28/08 to ACZ and EK06/11 to MBW). Informed individual donors provided written consent prior to sampling. Human naïve and memory B cells were enriched from PBMC preparations using the MACS B cell isolation kit II in combination with CD27 MicroBeads for human tissues (Miltenyi). For flow cytometry, experiments were performed in accordance with established guidelines [28]. Leukocyte suspensions were incubated with the indicated fluorochrome conjugated antibodies (see Supporting Information Table S1 for all antibodies) and acquired on a BD FACS Canto II flow cytometer. Cell populations were analyzed using BD FACS Diva software and FlowJo (Treestar) according to gating strategies as shown in Supporting Information Fig. S1.

Flow cytometry of ratiometric Ca^{2+} measurements

B cells from different sources were labeled separately with anti-B220 using donor-specific fluorescent conjugates (V450 or APC/Cy7) and mixed for further treatments and Ca^{2+} measurements within the same tube. Cells were additionally labeled with anti-CD21 (APC) to discriminate follicular from marginal zone B cells as shown in Supporting Information Fig. 1. Mixed cells were loaded with 1.3 $\mu\text{g}/\text{mL}$ Fluo-3 and 2.7 $\mu\text{g}/\text{mL}$ FuraRed (Life Tech-

nologies) in RPMI for 30 min at 37°C, then washed and incubated in standard Ringer's solution (155 mM NaCl, 4.5 mM KCl, 2 mM MgCl_2 , 10 mM D-glucose, 5 mM HEPES, pH 7.4), which either contained 1 mM CaCl_2 or 1 mM EGTA instead for measurements of Ca^{2+} release from internal stores. Fluo-3/FuraRed ratio was acquired on a BD FACSCanto II. BCR-specific response was induced after baseline recording in Ca^{2+} -containing buffer by addition of 10 $\mu\text{g}/\text{mL}$ of anti-IgM F(ab')₂. Ca^{2+} release from the ER was induced by 1 μM thapsigargin (Millipore) to irreversibly block SERCAs in Ca^{2+} -free buffer. To measure Ca^{2+} clearance following SOCE, thapsigargin-treated cells were washed to remove EGTA and resuspended in Ca^{2+} -containing Ringer's solution. High Ca^{2+} levels resulting from SOCE were recorded for 3 min. To monitor Ca^{2+} clearance, cells were centrifuged and resuspended in Ca^{2+} -free Ringer's solution and acquired immediately for additional 5 min. Ca^{2+} kinetics were analyzed using FlowJo kinetics tool and Excel.

For Ca^{2+} measurements in BM B-cell populations, total BM cells were labeled with anti-IgM APC, anti-B220 V450, and a dump mix containing anti-CD11b and anti-TCR- β APC/Cy7 antibodies. In this assay, cells from different donors could not be mixed, and were separately labeled with Fluo3 and FuraRed, and washed and resuspended in Ca^{2+} -free Ringer solution for measurement of ER Ca^{2+} release by addition of Tg as described above. BM B-cell populations were gated as depicted in Supporting Information Fig. 1. Area under the curve (AUC) either after addition of anti-IgM F(ab')₂ for 10 min, after addition of Tg for 10 min or after removal of extracellular Ca^{2+} for 5 min was calculated from the resulting mean kinetics curve of each donor cell population in each experiment using Excel software. AUC values in single experiments were normalized to the AUC of the corresponding WT control cells in the same experiment. In order to estimate the frequency of cells with extreme Ca^{2+} load, cells treated with Tg were first gated in a 3-min time interval around peak levels (1–4 min after addition of Tg). Cells with extreme Ca^{2+} load were then defined by having Fluo3/FuraRed ratios larger than 99.0% of the corresponding control cells for each experiment, and quantified as the mean frequency \pm SD.

Preparation of protein extracts from B cells and western blotting

Cell pellets were homogenized by incubation at 4°C for 30 min in Triton-homogenization buffer (20 mM Tris pH 7.5, 150 mM NaCl, 1% Triton-X-100, 2 mM MgCl_2 , 750 U/mL Benzonase (Sigma), and protease inhibitors (protease inhibitor cocktail tablets, Roche)), centrifuged at 15 000 g for 20 min, and the resulting supernatants were used for analysis. Protein content was determined using a bicinchoninic acid kit according to the manufacturer's instructions (ThermoFisher Pierce). Western blots were performed as described [8]. In brief, anti-PMCA1 and anti-PMCA4 antibodies (see Supporting Information Table S1) were used at 1:1000 and immunoreactivity was detected using an ECL imager (GeneGnome XRQ, Syngene, Cambridge, UK).

Estimation of relative levels of *Pmca1* and *Pmca4* mRNAs

Total RNA from mouse tissues was isolated using peqGold TriFast™ (peqlab, Erlangen, Germany) according to the manufacturer's instructions. Total RNA from purified mouse or human cells and cell lines was isolated using the NucleoSpin RNA Kit according to the manufacturer's instructions (Macherey Nagel, Düren, Germany). The analysis was performed according to a method published by Okunade et al. [27]. This strategy is based on first simultaneously amplifying *Pmca1* and *Pmca4* cDNA fragments, followed by gene-specific restriction digest of PCR products (as shown in Fig. 2D and E). First-strand cDNA was prepared using the RevertAid H Minus First Strand cDNA Synthesis Kit (Thermo Fisher Scientific). Briefly, 500 ng total RNA was reverse transcribed using random primers, followed by PCR using either the primers described in reference [27] (for mouse samples), or primers adapted to human sequences (forward primer 5'-GGTACCCATGTAATGGAAGGTTCTGG-3' corresponding to *Pmca1* codons 363–371 and *Pmca4* codons 259–267 and reverse primer 5'-ATGATCTCAGATGCGCCCTTGCTGAATAT-3' corresponding to *Pmca1* codons 598–607 and *Pmca4* codons 588–597 for X-splice variants in splice site A or 576–585 for Z-splice variants, respectively). The primers have two mismatches relative to each mRNA to allow for efficient amplification of *Pmca1* and *Pmca4*, but not *Pmca2* or *Pmca3*. PCR products were purified using the NucleoSpin Gel and PCR clean-up Kit (Macherey Nagel), followed by restriction digests of 400 ng purified PCR product with the enzymes specified in Fig. 2 (Fast Digest Enzymes, Thermo Fisher Scientific).

PCR of genomic DNA from sorted B-cell populations and DCs

Splenic FOBs and MZBs and BM B cell populations were sorted on BD FACS Aria III according to gating strategies shown in Supporting Information Fig. 1A and D. BM-derived DCs were generated by a 9-day culture of BM cells in the presence of GM-CSF. Genomic DNA from purified cell populations was prepared using the Nucleo Spin Tissue Kit according to the manufacturer's instructions (Macherey Nagel, Düren, Germany). Equal nanogram amounts (~70 ng) of genomic DNA were used for all PCRs. Based on the PCR strategy given by the KOMP repository (www.mmrrc.org, KOMP Project ID CSD77635, MMRRC stock #: 046724-UCD), PCR was performed using the following primers: CSD-Atp2b1-F (5'-CTAGGCATATAATGGGCGAAGCAGC-3' located in the 5'-arm of the KO construct) and CSD-Atp2b1-R (5'-CCAGATGGCATGTCTCAACATCAGC-3' located in the 3'-arm). The expected amplicon of 750 bp is indicative of the PostFlp & Cre genotype. PCR conditions were adapted by prolonging the synthesis step to 2 min, thus allowing parallel synthesis of 1639 bp PostFlp and/or 1434 bp WT genotype. Amplification products were separated by gel electrophoresis and fragment band inten-

sities were quantified using GeneTools, version 3.07 (SynGene, Cambridge, UK).

Statistical analysis

Statistical significance was determined by unpaired Student's two-tailed *t*-tests or one-way ANOVA tests as indicated using Excel or GraphPad Prism version 7, respectively.

Acknowledgements: The authors thank Roland Hartig for cell sorting by flow cytometry, and Stefanie Holze and Christoph Schwarzer for excellent technical assistance. This work was supported by the Deutsche Forschungsgemeinschaft grant SFB854-B08 to K.D.F. and U.T., SFB854-B14 to M.B.-W., and by the ABINEP graduate school funded by the Ministry for Economics, Science, and Digitization of the State Sachsen-Anhalt to K.D.F. Open access funding enabled and organized by Projekt DEAL.

Conflict of interest: The authors declare that they have no financial or commercial conflict of interest.

Peer review: The peer review history for this article is available at <https://publons.com/publon/10.1002/eji.202048654>.

Data availability statement: The data that support the findings of this study are available from the corresponding author upon reasonable request.

References

- Hemon, P., Renaudineau, Y., Debant, M., Le Goux, N., Mukherjee, S., Brooks, W. and Mignen, O., Calcium signaling: from normal B cell development to tolerance breakdown and autoimmunity. *Clin. Rev. Allergy Immunol.* 2017. 53: 141–165.
- Cali, T., Brini, M. and Carafoli, E., Regulation of cell calcium and role of plasma membrane calcium ATPases. *Int. Rev. Cell. Mol. Biol.* 2017. 332: 259–296.
- Krebs, J., The plasma membrane calcium pump (PMCA): regulation of cytosolic Ca(2+), genetic diversities and its role in sub-plasma membrane microdomains. *Adv. Exp. Med. Biol.* 2017. 981: 3–21.
- Hegedus, L., Zambo, B., Paszty, K., Padanyi, R., Varga, K., Penniston, J. T. and Enyedi, A., Molecular diversity of plasma membrane Ca(2+) transporting ATPases: their function under normal and pathological conditions. *Adv. Exp. Med. Biol.* 2020. 1131: 93–129.
- Strehler, E. E., Plasma membrane calcium ATPases: from generic Ca(2+) sump pumps to versatile systems for fine-tuning cellular Ca(2+). *Biochem. Biophys. Res. Commun.* 2015. 460: 26–33.
- Chen, J., Sitsel, A., Benoy, V., Sepulveda, M. R. and Vangheluwe, P., Primary active Ca(2+) transport systems in health and disease. *Cold Spring Harb. Perspect. Biol.* 2020.12. <https://doi.org/10.1101/cshperspect.a035113>

- 7 Strehler, E. E., Plasma membrane calcium ATPases as novel candidates for therapeutic agent development. *J. Pharm. Pharm. Sci.* 2013. **16**: 190–206.
- 8 Korthals, M., Langnaese, K., Smalla, K. H., Kahne, T., Herrera-Molina, R., Handschuh, J., Lehmann, A. C. et al., A complex of neuroplastin and plasma membrane Ca(2+) ATPase controls T cell activation. *Sci. Rep.* 2017. **7**: 8358.
- 9 Go, C. K., Hooper, R., Aronson, M. R., Schultz, B., Cangoz, T., Nemani, N., Zhang, Y. et al., The Ca(2+) export pump PMCA clears near-membrane Ca(2+) to facilitate store-operated Ca(2+) entry and NFAT activation. *Sci. Signal* 2019. **12**. <https://doi.org/10.1126/scisignal.aaw2627>
- 10 Kim, B., Takeuchi, A., Hikida, M. and Matsuoka, S., Roles of the mitochondrial Na(+)-Ca(2+) exchanger, NCLX, in B lymphocyte chemotaxis. *Sci. Rep.* 2016. **6**: 28378.
- 11 Chen, J., McLean, P. A., Neel, B. G., Okunade, G., Shull, G. E. and Wortis, H. H., CD22 attenuates calcium signaling by potentiating plasma membrane calcium-ATPase activity. *Nat. Immunol.* 2004. **5**: 651–657.
- 12 Schmidt-Suppran, M. and Rajewsky, K., Vagaries of conditional gene targeting. *Nat. Immunol.* 2007. **8**: 665–668.
- 13 Horcher, M., Souabni, A. and Busslinger, M., Pax5/BSAP maintains the identity of B cells in late B lymphopoiesis. *Immunity* 2001. **14**: 779–790.
- 14 Lyszkiewicz, M., Kotlarz, D., Ziętara, N., Brandes, G., Diestelhorst, J., Glage, S., Hobeika, E. et al., LAMTOR2 (p14) controls B cell differentiation by orchestrating endosomal BCR trafficking. *Front. Immunol.* 2019. **10**: 497.
- 15 Rickert, R. C., Roes, J. and Rajewsky, K., B lymphocyte-specific, Cre-mediated mutagenesis in mice. *Nucleic Acids. Res.* 1997. **25**: 1317–1318.
- 16 Bautista, D. M., Hoth, M. and Lewis, R. S., Enhancement of calcium signalling dynamics and stability by delayed modulation of the plasma-membrane calcium-ATPase in human T cells. *J. Physiol.* 2002. **541**: 877–894.
- 17 Casola, S., Control of peripheral B-cell development. *Curr. Opin. Immunol.* 2007. **19**: 143–149.
- 18 Pillai, S. and Cariappa, A., The follicular versus marginal zone B lymphocyte cell fate decision. *Nat. Rev. Immunol.* 2009. **9**: 767–777.
- 19 Hao, Z. and Rajewsky, K., Homeostasis of peripheral B cells in the absence of B cell influx from the bone marrow. *J. Exp. Med.* 2001. **194**: 1151–1164.
- 20 Savage, H. P., Kläsener, K., Smith, F. L., Luo, Z., Reth, M. and Baumgarth, N., TLR induces reorganization of the IgM-BCR complex regulating murine B-1 cell responses to infections. *Elife* 2019. **8**. <https://doi.org/10.7554/eLife.46997>
- 21 Heng, T. S. and Painter, M. W., The Immunological Genome Project: networks of gene expression in immune cells. *Nat. Immunol.* 2008. **9**: 1091–1094.
- 22 Curry, M. C., Luk, N. A., Kenny, P. A., Roberts-Thomson, S. J. and Monteith, G. R., Distinct regulation of cytoplasmic calcium signals and cell death pathways by different plasma membrane calcium ATPase isoforms in MDA-MB-231 breast cancer cells. *J. Biol. Chem.* 2012. **287**: 28598–28608.
- 23 Johnston, H. E., Carter, M. J., Larrayoz, M., Clarke, J., Garbis, S. D., Oscier, D., Strefford, J. C. et al., Proteomics profiling of CLL versus healthy B-cells identifies putative therapeutic targets and a subtype-independent signature of spliceosome dysregulation. *Mol. Cell. Proteomics* 2018. **17**: 776–791.
- 24 Ribiczey, P., Papp, B., Homolya, L., Enyedi, A. and Kovacs, T., Selective upregulation of the expression of plasma membrane calcium ATPase isoforms upon differentiation and 1,25(OH)2D3-vitamin treatment of colon cancer cells. *Biochem. Biophys. Res. Commun.* 2015. **464**: 189–194.
- 25 Gwack, Y., Srikanth, S., Oh-Hora, M., Hogan, P. G., Lamperti, E. D., Yamashita, M., Gelinis, C. et al., Hair loss and defective T- and B-cell function in mice lacking ORAI1. *Mol. Cell. Biol.* 2008. **28**: 5209–5222.
- 26 Matsumoto, M., Fujii, Y., Baba, A., Hikida, M., Kurosaki, T. and Baba, Y., The calcium sensors STIM1 and STIM2 control B cell regulatory function through interleukin-10 production. *Immunity* 2011. **34**: 703–714.
- 27 Okunade, G. W., Miller, M. L., Pyne, G. J., Sutliff, R. L., O'Connor, K. T., Neumann, J. C., Andringa, A. et al., Targeted ablation of plasma membrane Ca2+-ATPase (PMCA) 1 and 4 indicates a major housekeeping function for PMCA1 and a critical role in hyperactivated sperm motility and male fertility for PMCA4. *J. Biol. Chem.* 2004. **279**: 33742–33750.
- 28 Cossarizza, A., Chang, H. D., Radbruch, A., Acs, A., Adam, D., Adam-Klages, S., Agace, W. W. et al., Guidelines for the use of flow cytometry and cell sorting in immunological studies (second edition). *Eur. J. Immunol.* 2019. **49**: 1457–1973.

Abbreviations: **FOB:** follicular B cell · **MZB:** marginal zone B cell · **PMCA:** plasma membrane Ca²⁺ ATPase · **SERCA:** sarco/endoplasmic reticulum Ca²⁺ ATPase · **SOCE:** store-operated calcium entry · **Tg:** thapsigargin

Full correspondence: Dr. Klaus-Dieter Fischer, Institute for Biochemistry and Cell Biology, Otto-von-Guericke University, Leipziger Str. 44, Magdeburg 39120, Germany
e-mail: klaus.fischer@med.ovgu.de

Received: 26/3/2020

Revised: 29/8/2020

Accepted: 22/10/2020

Accepted article online: 24/10/2020